Final Draft
of the original manuscript:

Wen, T.; Wang, H.-F.; Georgopanos, P.; Avgeropoulos, A.; Ho, R.-M.:
Three-dimensional visualization of phase transition in polystyrene-block-polydimethylsiloxane thin film.
In: Polymer. Vol. 167 (2019) 209 - 214.
First published online by Elsevier: 21.01.2019

https://dx.doi.org/10.1016/j.polymer.2019.01.047

Three-Dimensional Visualization of Phase Transition in Polystyrene-*block*-Polydimethylsiloxane Thin Film

Tao Wen [a,b*], Hsiao-Fang Wang [b], Prokopios Georgopanos [c,d], Apostolos Avgeropoulos [c] and Rong-Ming Ho [b*]

[a] South China Advanced Institute for Soft Matter Science and Technology, South China University of Technology, Guangzhou, 510640

[b] Department of Chemical Engineering, National Tsing Hua University, Hsinchu, 30013

[c] Department of Materials Science and Engineering, University of Ioannina, University Campus Ioannina 45110, Greece

d Helmholtz-Zentrum Geesthacht, Institute of Polymer Research, Max-Planck-Straße 1, 21502, Geesthacht, Germany

Abstract

Herein, we aim to examine the order-order transition (OOT) of self-assembled block copolymer (BCP) under spatial confinement using double gyroid (DG) structured polystyrene-*block*-polydimethylsiloxane (PS-PDMS) thin film as an exemplary system for three-dimensional (3D) visualization of phase transitions. An interesting OOT from DG to hexagonally perforated lamellae (HPL) can be found after thermal annealing, and the morphological evolution and corresponding mechanism for the OOT was systematically investigated by 3D transmission electron microscopy (3D TEM). Our results revealed that the phase transition of DG nanostructure in thin film was different from that in bulk, which is attributed into the surficial/interfacial effects and the effect of confinement on BCP self-assembly. This work provides a feasible method to prepare DG-nanostructured thin film and presents a model system for the examination of morphological evolution from metastable to phase with higher thermodynamic stability in the thin-film state through the OOT.

Keywords: block copolymer, self-assembly, phase transition, 3D TEM, order-order transition

TOC image

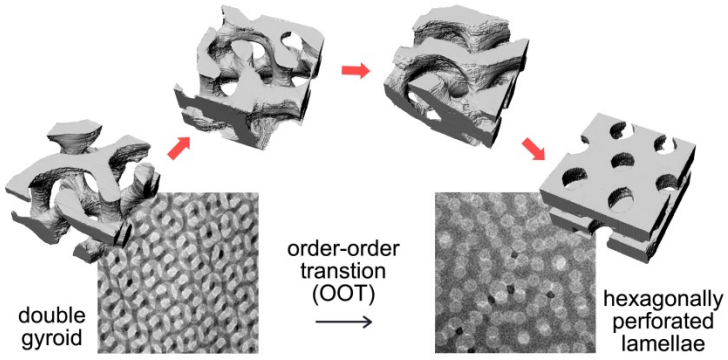
double
gyroid
order-order
transtion
(OOT)
hexagonally
perforated
lamellae

1. Introduction

Block copolymers (BCPs) composed of two incompatible blocks can self-assemble into a variety of ordered phases [1-4]. The thermodynamically stable phase results from the balance between maximizing conformational entropy and minimizing interaction energy of incompatible blocks. In practical applications, the self-assembled phases of BCPs are usually achieved by solution casting. In this case, the affinity between solvent and the constituent blocks would affect the self-assembly of BCPs, and results in the formation of metastable phases [5-10]. The transition of the metastable phase into thermodynamically stable phase could take place with the inducement of temperature variation (thermal annealing) or external fields [11-14]. Such order-order transitions (OOTs) between different phases have been extensively studied theoretically and experimentally [6, 15-24]. Among various OOTs of BCPs, the transitions involving double gyroid phase (DG) with a space group of $Ia\bar{3}d$, are of importance. Note that DG is a three-dimensional (3D) network whereas lamellar phase (L) and cylinder phase (C) are one-dimensional (~~2D~~1D) and two-dimensional (~~1D~~2D) structure, respectively [25-29]. The structural and morphological evolution takes place in OOT is usually examined by combining small-angle X-ray scattering (SAXS) and transmission electron microscopy (TEM). However, the corresponding results could only provide limited information with respect to the details of phase transition mechanism. For one thing, the scattering measurement gives averaged morphological information but is lack of the details of the textures. For another, conventional TEM image might provide the structural details but it is difficult to examine complicate 3D morphologies since it is a 2D projection for 3D object. To address this problem, 3D TEM has been developed to directly visualize the self-assembled phases of BCPs in real space [30, 31]. As most of the studies focused on OOT took place in the bulk state, the reports of OOT arising in thin film have been rarely studies. Compared with that of bulk samples, the phase behaviors of thin-film BCPs are expected to be much more complex because the microphase separated morphologies would be significantly influenced by the film thickness (*i.e.*, spatial confinement) and surface energetics [32]. Compared with that in bulk, the

understanding of the OOT of DG phase in thin film is of importance due to its potential in optical applications, such as antireflection coatings and photonic crystals [33, 34]. However, it is still challenging to achieve well-defined DG thin film with a thickness close to its long period (or lattice size) [35-38].

In our previous studies, DG phase of a lamella-forming polystyrene-*block*-polydimethylsiloxane (PS-PDMS) BCP can be simply obtained by the selectivity of solvent [39]. The strong segregation strength of the PS-PDMS leads to the formation of clear-cut phase with extremely high structural ordering. In the present case, slices of PS-PDMS were prepared by using cryo-ultramicrotome from solution-cast bulk, giving highly ordered DG-structured thin film as an ideal model system for the examination of morphological evolution of DG phase under spatial confinement. Note that it is easier to acquire the one with the (211) in-plane orientation during microsectioning, due to the maximal area fraction of (211) plane in DG nanostructures [37]. Subsequently, the OOT of DG-structured PS-PDMS can be induced by thermal annealing after the slices were transferred onto TEM grids. Also, in the case of thin film, the interfacial effects play a vital role and strongly influence the OOT mechanism, especially in PDMS-containing BCPs at which the low surface energy of PDMS tends to wet the free surface [40]. With the use of carbon-coated substrate that can drive the formation of PS thin layer, the structural transition of DG in the slice can thus be confined to occur along the vertical direction and driven by the interfacial effects as built thermodynamically. With the examination of 3D TEM, the tomographic results for the OOT of the DG in thin film is expected to provide an exemplary system as compared with that in bulk, giving new insights into the understanding of the surface-induced motif shifts of complicate self-assembled morphologies and corresponding transition mechanisms.

2. Materials and methods

2.1 Polymer synthesis

The synthesis of PS-PDMS was carried out through sequential anionic polymerization of styrene and hexamethylcyclotrisiloxane using high vacuum

techniques. The reaction was carried out by using benzene and THF as solvents, *sec*-BuLi as an initiator, and trimethylchlorosilane ($ClSi(CH_3)_3$) as a termination reagent. The molecular characterization was carried out by using gel permeation chromatography (GPC) and ^1H nuclear magnetic resonance (NMR) spectroscopy. The number-average molecular weights of the PS and the PDMS in the PS-PDMS were 43.5 kg/mol and 29.0 kg/mol, respectively, as determined by the GPC analysis. The PDI of the PS-PDMS was determined as 1.04. The volume fraction of the PDMS block was calculated as 0.40 by assuming the densities of PS and PDMS are 1.02 and 0.97 g/cm^3, respectively [39].

2.2 Sample preparation.

The bulk sample of PS-PDMS was prepared by casting from toluene solution. The solvent evaporation for casting was carried out for approximately one week. The obtained samples were further dried in vacuum oven at ambient temperature to remove the residual solvent. The as-cast samples were sectioned by ultra-cryomicrotomy at -160 °C (thickness ~150 nm) for electron tomography. The microsections were collected onto copper grids (150 mesh) with carbon/poly(vinyl formal) supporting film. To induce the transition of metastable phase, the slices of PS-PDMS on the girds were thermally annealed at 180 °C for certain periods. The annealed samples were directly quenched in liquid nitrogen for electron tomography observation.

2.3 Tomography for reconstruction images

For the requirement of image alignment to reconstruct 3D imaging, fiducial gold markers (diameter 10 nm, purchased from Polysciences, Inc.) were used and homogeneously distributed onto the microsections with the right amount of markers to observe transition zone. Subsequently, a series of TEM projection images were collected from - 70 ° to + 70 ° tilt angles with an angular interval of 1 ° on a JEOL (JEM-2100) TEM operated at 200 kV. Images were recorded by a Gatan CCD camera. Alignment of the tilt series and 3D reconstruction were performed by using IMOD software. The reconstructed volume was then filtered by a 5×5×5 median filter for noise reduction. ImageJ-Fiji was then used to trim the filtered volume keeping only a

volume of interest for further analysis. Finally, 3D analyses such as binarization, segmentation, and visualization of the volume of interest were achieved by using 3D Slicer.

3. Results and discussion

3.1 OOT of PS-PDMS slices

Figure 1a shows the TEM micrograph of as-microtomed PS-PDMS slice, in which the dark and the bright regions represent PDMS and PS microdomains, respectively. In Figure 1a, a bicontinuous PDMS network with triple periods can be observed, which is a typical feature of DG nanostructure. However, it is challenging to index the lattice plane from 2D micrograph, because it could result from a complex projection, which is dependent both on the section thickness and the orientation of domains (see below for details). As reported previously, the achieved DG phase of as-cast PS-PDMS by solvent induction is a metastable phase, and thus, OOT of BCP, *i.e.*, DG → L, will take place in bulk under thermal annealing [39]. To examine such phase-transition behavior of DG phase in a confined space, the microtomed slice on TEM grids was thermally annealed at 180 °C for 60 min. As evidenced by *in-situ* SAXS results, this is long enough for the BCP to reach a much more stable phase due to the strong segregation strength between PS and PDMS [39]. Figure 1b shows the TEM micrograph of annealed PS-PDMS slice. Instead of usual L phase in bulk, bright spherical microdomains of PS in the PDMS matrix were found in the annealed slices. The PS microdomains have homogeneous sizes of approximately 50 nm but the arrangement of those microdomains could not be clearly identified in conventional TEM imaging.

3.2 Morphologies of annealed thin films

To further examine the morphologies of annealed slices and truly examine the phase transition mechanisms, 3D TEM was carried out to directly visualize the 3D nanostructure of the annealed PS-PDMS. Figures 2a and 2b show the reconstructed image and the digitally sliced images of PS-PDMS annealed at 180 °C for 60 min, at

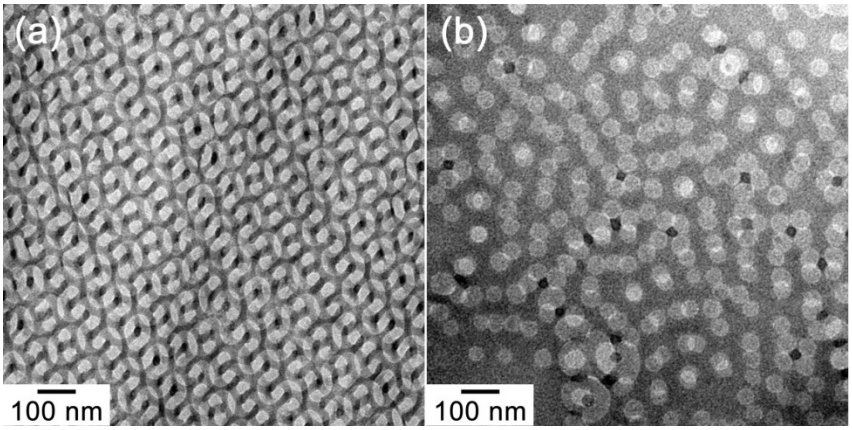

Figure 1. TEM micrographs of as-cast PS-PDMS from toluene solution without staining (a) before thermal annealing; (b) after thermal annealing at 180 °C for 60 min.

which the PS microdomains with a hexagonal packing can be clearly observed. It reveals that the channels extending through the minority component domain adopted a hexagonal symmetry. It indicates that the morphology shown in Figure 1b is attributed to the formation of double-layered hexagonally perforated lamellae (HPL), which is a long-lived non-equilibrium state of self-assembled BCPs [41]. This observation reveals that HPL structure of PS-PDMS can be achieved after long-time thermal annealing in the thin film. On the basis of the reconstructed results, the geometric parameters of HPL structure are allowed to be precisely measured. The average radius of PS domains and the inter-domain distance are approximately 23.8 and 45.1 nm, respectively. In addition, the reconstructed results indicate that there are two perforated PDMS layers oriented parallel to the substrate in the annealed slice. Figure 2c shows the reconstructed images of the two perforated PDMS layers, *i.e.*, top layer (close to free surface, marked as blue) and bottom layer (close to substrate, marked as green). Hexagonally packed perforations can be clearly observed in each layer, indicating the homogeneity of phase structure after annealing. Yet, the relative positions of perforations in these two respective layers were not identical, resulting in the overlapped projection of the two layers with different packing orientation (*i.e.*, a non-distinguishable symmetry) (Figure 1b). We speculate that this is attributed to the re-organization of up- and bottom-perforated layers during phase transition, and this

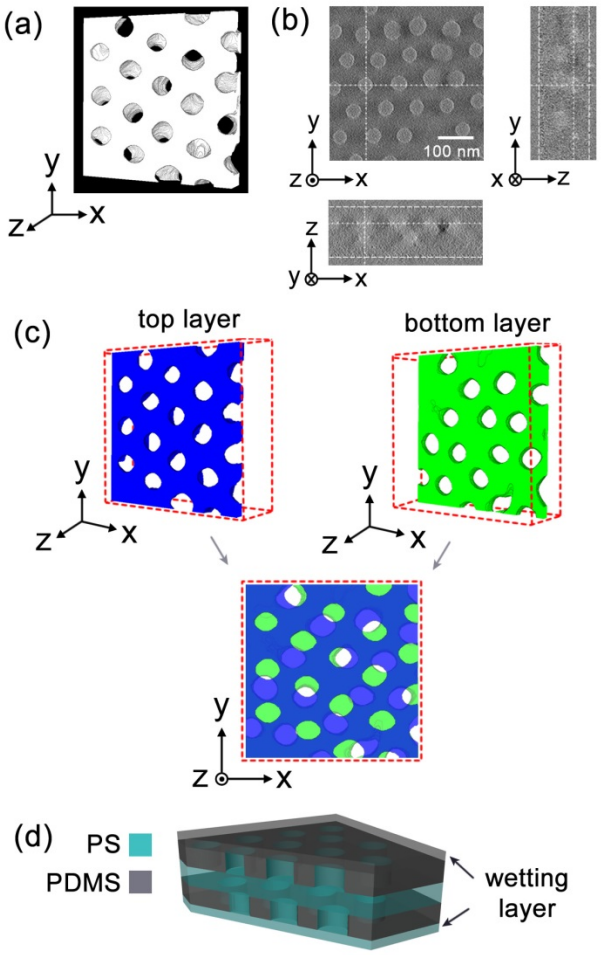

Figure 2. (a) 3D reconstruction image and (b) digitally sliced images of PS-PDMS thin film after thermal annealing at 180 °C for 60 min. (c) Self-assembled morphologies near the top PDMS and the bottom PS in the annealed thin film. (d) Schematic illustration of HPL structure forming under spatial confinement after long-time thermal annealing.

will be discussed later. Similar result was also observed in the self-assembled thin film of polystyrene-*block*-polyisoprene (PS-PI), in which the perforations have different structural types between the neighbor HPL layers [42].

3.3 Structural evolution of DG under confinement

As evidenced above, HPL phase was formed by PS-PDMS DG thin film after long-time thermal annealing. To further investigate the mechanism of observed OOT in thin film, the morphological evolution of PS-PDMS slices with different annealing periods was studied at different transition stages. Figure 3 shows the reconstructed

result of DG phase of as-microtomed PS-PDMS slice along the given directions, at which two interpenetrating PDMS networks can be observed (Figure 3a). Figure ~~2b~~3b shows the digitally sliced images of the orthogonal planes of the as-cast PS-PDMS. The cross sectional view exhibits a characteristic “double-wave” pattern, indicating that the microtomed slice cuts parallel to the (211) plane of the DG structure (Figure 3b) [43]. Also, the thickness of as-microtomed slice measured from the cross-view of reconstructed image was approximately 155 nm, which is equal to the cubic size as mentioned above. In the as-microtomed slice, two alternative PDMS networks results in an overlapping projection in conventional TEM micrograph as shown in Figure 1a. As previously reported, there is an epitaxial relation between the (211) plane of DG and the (10) plane of HPL during the phase transition from DG to HPL in bulk sample [17, 39, 44, 45]. As shown in Figure 2, the (10) plane of HPL phase in the annealed slice is parallel to the substrate. That means the DG transformed into a HPL phase with a flat-on orientation, which differs from the OOT occurs in bulk. To achieve the detailed information of the transition process, the morphologies of slices annealed for different periods were examined by 3D TEM.

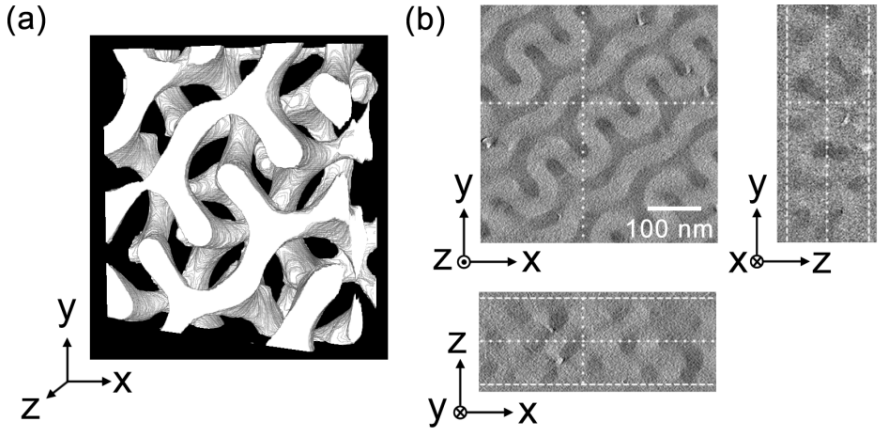

Figure 3. (a) 3D reconstruction image and (b) digitally sliced images of PS-PDMS thin film cast from toluene solution.

Figure 4a shows the TEM micrograph of PS-PDMS slice annealed at 180 °C for 2 min at which the morphology with tetragonally packed PS microdomains can be observed (Figure 4a). It indicates that a rapid transition of DG nanostructure in thin film was induced by thermal annealing. In fact, the transition in bulk sample is slower

than that in thin film [39]. For thin film, the surficial/interfacial effect is a critical constraint. To minimize the energy of system, one of the blocks possessing lower surficial or interfacial energy will be preferentially wet the free surface and the interface, *i.e.*, selective wetting. Such selective wetting can lead to the quantization of film thickness [32, 46, 47]. The average thickness of as-microtomed slices (L) after annealing is approximately 155 nm, whereas the annealed slice is slightly thinner than the as-microtomed one (approximately 150 nm), due to the creeping at annealing temperature. The spacing of the intrinsic L phase of PS-PDMS (L_0) in this study is approximately 61 nm [39]. Namely, the thickness of as-microtomed slice is about 2.5 times the spacing of the intrinsic lamellar phase, $L \approx (n + 0.5) L_0$, where n is an integer. The reconstructed image reveals that no surficial topography with characteristic one L_0 step heights formed during thermal annealing, which suggesting the occurrence of asymmetric wetting in the PS-PDMS slice during thermal annealing [32]. Namely, PDMS and PS would preferentially wet the air/polymer interface and the polymer/substrate interface, respectively. This result is consistent with our previous study [40]. Under annealing temperature, the generation of wetting layer and phase transition takes place simultaneously. However, the formation of wetting layer is expected to be faster than the OOT process. We speculate that the fast kinetics of OOT in thin film is attributed to the formation of wetting layer, which provides additional driving force to the OOT.

Figure 4c shows the corresponding 3D reconstruction image of annealed slice for 2 min, in which a deformed PDMS skeleton can be observed. It confirms that the quasi-tetragonal projection in Figure 4a is attributed into such deformation of bicontinuous PDMS networks. As the temperature above the glass transition temperature (T_g) of PS matrix, DG nanostructures was compressed along the vertical direction of slice. In the virginal nanostructure of the microtomed slice, the bicontinuous network of DG is constructed by the connected tripods with a dihedral angle of 70.5° [18, 48]. Under thermal annealing, the rotated tripods were compressed along the normal direction, and gradually transferred into a planar structure with the dihedral angle close to 0 ° (Figure 4e). Actually, an reversed transition of the dihedral

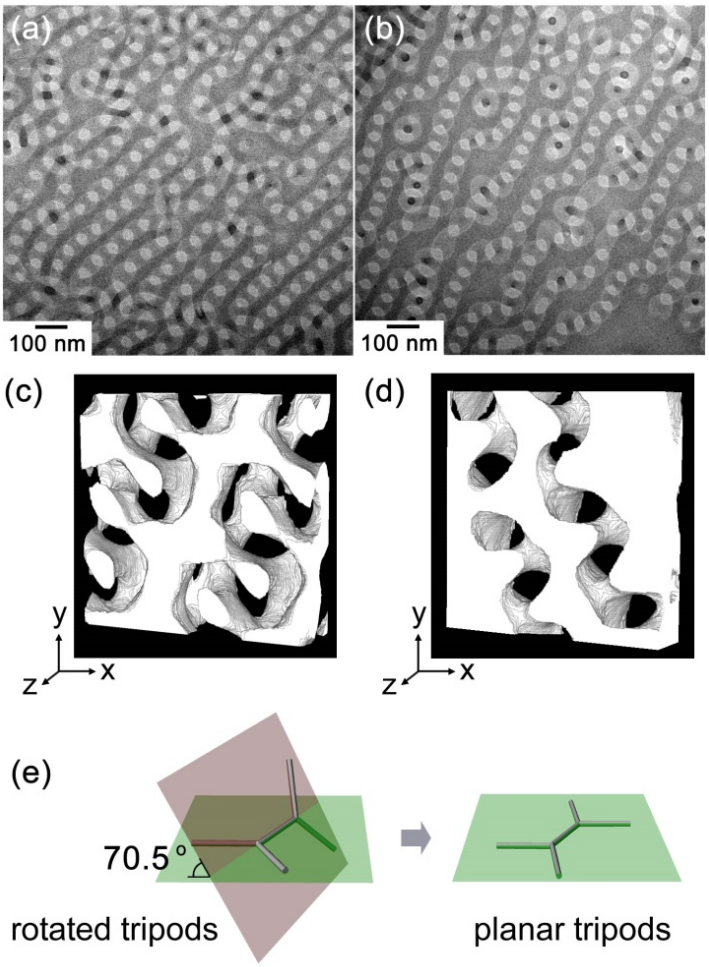

Figure 4. TEM micrographs and 3D reconstruction images of PS-PDMS thin film annealed at 180 °C for 2 min (a and c) and 10 min (b and d). Schematic illustration of the rotated tripods in DG phase and the planar tripods after thermal annealing.

angle of tripods (from 0 ° to 70.5 °) can be found in the OOT of HPL to DG [49]. It suggests that the structural transition between DG and HPL would consistently arise along this topological pathway. As mentioned, however, the transition of the tripods can be only allowed to take place along the <211> axis due to the fixed orientation of the slice. As a result, the crossing angle of the final planar tripods is dependent on the initial orientation of the slice. By contrast, the corresponding crossing angle of planar tripods is 120 ° in bulk based on the theoretical prediction [49]. Although the deformation of DG ~~nanostrcutures~~ nanostructures can be occurred after a short-time annealing, two mutually interwoven PDMS domains were still separated from each other. Figures 4b and 4d show the TEM micrograph and the corresponding

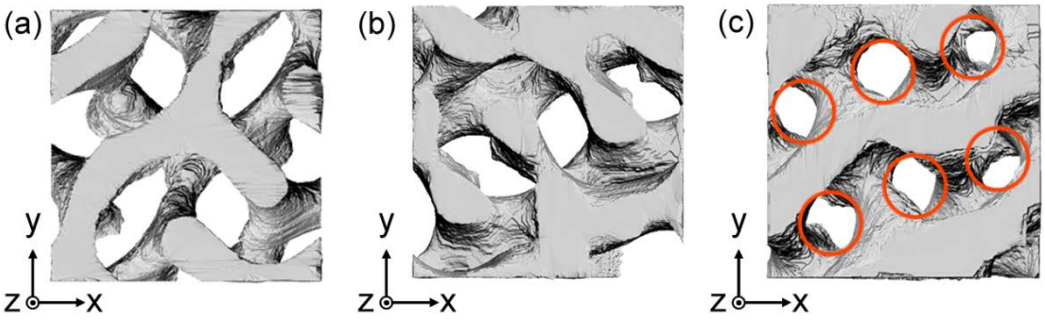

Figure 5. 3D segmented PDMS networks viewed along the vertical direction of PS-PDMS thin film thermally annealed for different time (a) 0 min; (b) 2 min; (c) 10 min.

reconstructed results of the PS-PDMS slice annealed at 180 ° for 10 min. With further increasing of annealing time, the merging of the two networks gradually took place. As shown in the TEM projection, the elongation of annealing time led to the transition of the 3D skeleton of DG to a planar structure. The reconstructed image reveals that the merging of two PDMS networks giving rise to the formation of planar nanostructures, and the PS microdomains were gradually divided into separated microdomains by the merged PDMS networks.

The 3D images of PS-PDMS slices at different transition stages viewing along the normal direction are summarized in Figure 5, in which the evolution of structural symmetry upon thermal annealing can be clearly observed. In the as-microtomed slice, two interwoven networks exhibited a hexagonal symmetry. The softening of PS matrix leads to a deformed and compressed PDMS network under thermal annealing, and the merged network of PDMS give rise to a quasi-tetragonal symmetry of divided PS domains, as indicated by the ~~cycles~~ circles in Figure 5c. This is an intermediate structure determined by the initial orientation of rotated tripods in the as-microtomed slice. However, hexagonally packed perforation is much more stable than that with a tetragonal packing for perforated lamellar structures [50]. As a result, the quasi-tetragonal packing of PS domains would eventually transfer into hexagonal packed structures. In addition, it was found the perforations in the two layers are different, and there is no simple correlation between upper and bottom layers. We speculate that the quasi-tetragonal structures reorganized independently in each of the

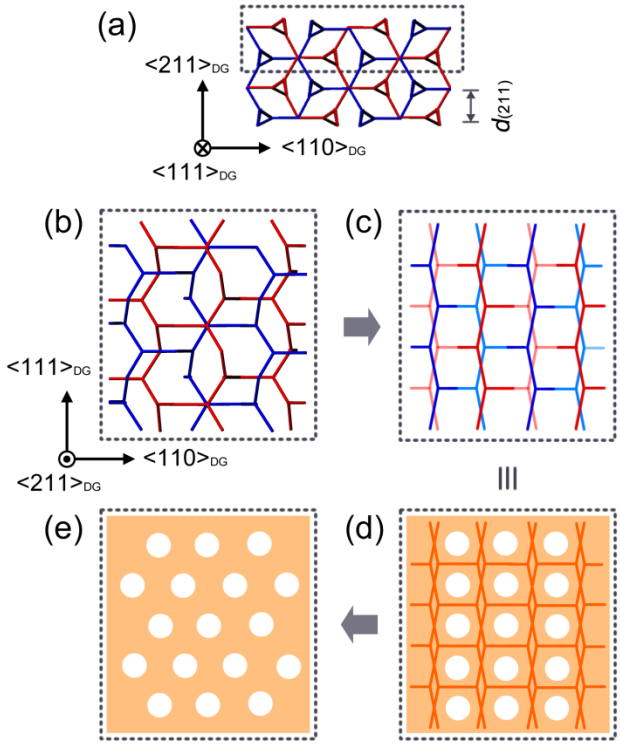

Figure 6. Illustrations of DG phase in the PS-PDMS thin film before annealing which are parallel to the (211) plane (a: side view; b: top view). The deformed and compressed PDMS networks led to a quasi-tetragonal symmetry of PS domains (c and d), which would finally transfer to HPL phase. For clarity, only top half of the slice, marked by the box in (a), was shown.

layers. As a result, the final packing patterns of PS microdomains in HPL are distinct in the two layers. Compared with bulk sample, the wetting effects and the special confinement give rise to a distinct OOT of DG nanostructure in thin film. In bulk, the (10) plane of L nucleates and epitaxially grows from the (211) plane of DG, and this transition has to intermediate with a multiple-layer structure, due to the mismatching in the lattices for the DG to L [39]. Our observation indicates that the structural transition along the direction normal to the thin film (z-direction) is much faster than that along in-plane directions (x- and y-direction).

Figure 6 shows a schematic representation of OOT in microtomed slice with DG nanostructure. Note that the lattice spacing of the (211) plane of DG phase is approximately 52.8 nm, which means three periods of (211) plane were involved in the slice (Figure 6a) [39]. In the initial slice, the (211) plane of DG phase is parallel to

the substrate. Owing to the surficial/interfacial effects and the thickness confinement, the phase transition of DG primarily arose along the normal direction, *i.e.*, <211> axis (Figures 6b and 6c). In the early stage of thermal annealing, the deformation and merging of rotated PDMS tripods gradually leads to the formation of intermediate phase with a quasi-tetragonal packing, which is determined by the initial orientation of DG nanostructure (Figure 6d). With further annealing, the rearrangement of the metastable phase gave rise to a HPL phase with higher thermodynamic stability after long-time annealing (Figure 6e).

4. Conclusions

In the present work, the OOT of PS-PDMS BCPs with an initial DG phase in microtomed slices was studied. Compared with OOT occurs in bulk, the long-life metastable (HPL phase) can be formed in microtomed slices by thermal annealing, instead of the intrinsic stable phase (L phase). Owing to the surficial and interfacial effects, as well as the thickness confinement, the phase transition in microtomed slice was induced to proceed along the vertical direction, which is different from the OOT in bulk where the epitaxial relation is always kept between two phases. Also, the initial orientation of the ordered structure in thin film or microtomed slice could impact the pathway of phase transition process. The present work develops a feasible method to study the OOT behaviors of DG nanostructure in thin film, and the corresponding results provide new insights into the phase transitions of BCPs.

Acknowledgements:

TW thanks the financial supports from the National Natural Science Foundation of China (Grant No. 21803020), the Program for Guangdong Introducing Innovative and Entrepreneurial Teams (No.2016ZT06C322) and the startup support from the South China University of Technology.

References:

[1] F. S. Bates and G. H. Fredrickson. Block copolymer thermodynamics: theory and experiment, Annu. Rev. Phys. Chem. 41 (1990):525-557.

[2] M. W. Matsen and F. S. Bates. Unifying weak- and strong-segregation block copolymer theories, Macromolecules 29 (1996):1091-1098.

[3] C. Park, J. Yoon, and E. L. Thomas. Enabling nanotechnology with self assembled block copolymer patterns, Polymer 44 (2003):6725-6760.

[4] T.-Y. Lo, M. R. Krishnan, K.-Y. Lu, and R.-M. Ho. Silicon-containing block copolymers for lithographic applications, Prog. Polym. Sci. 77 (2018):19-68.

[5] N. P. Balsara, D. Perahia, C. R. Safinya, M. Tirrell, and T. P. Lodge. Birefringence detection of the order-to-disorder transition in block copolymer liquids, Macromolecules 25 (1992):3896-3901.

[6] D. A. Hajduk, S. M. Gruner, P. Rangarajan, R. A. Register, L. J. Fetters, C. Honeker, R. J. Albalak, and E. L. Thomas. Observation of a reversible thermotropic order-order transition in a diblock copolymer, Macromolecules 27 (1994):490-501.

[7] S. Sakurai, T. Hashimoto, and L. J. Fetters. Thermoreversible cylinder-sphere transition of polystyrene-*block*-polyisoprene diblock copolymers in dioctyl phthalate solutions, Macromolecules 29 (1996):740-747.

[8] K. J. Hanley, T. P. Lodge, and C.-I. Huang. Phase behavior of a block copolymer in solvents of varying selectivity, Macromolecules 33 (2000):5918-5931.

[9] C. Lai, W. B. Russel, and R. A. Register. Phase behavior of styrene-isoprene diblock copolymers in strongly selective solvents, Macromolecules 35 (2002):841-849.

[10] T.-Y. Lo, C.-C. Chao, R.-M. Ho, P. Georgopanos, A. Avgeropoulos, and E. L. Thomas. Phase transitions of polystyrene-*b*-poly(dimethylsiloxane) in solvents of varying selectivity, Macromolecules 46 (2013):7513-7524.

[11] E. L. Thomas, D. B. Alward, D. J. Kinning, D. C. Martin, D. L. Handlin, and L. J. Fetters. Ordered bicontinuous double-diamond structure of star block copolymers: a new equilibrium microdomain morphology, Macromolecules 19 (1986):2197-2202.

[12] S. Sakurai, T. Momii, K. Taie, M. Shibayama, S. Nomura, and T. Hashimoto. Morphology transition from cylindrical to lamellar microdomains of block copolymers, Macromolecules 26 (1993):485-491.

[13] M. W. Matsen and F. S. Bates. Block copolymer microstructures in the

intermediate-segregation regime, J. Chem. Phys. 106 (1997):2436-2448.

[14] U. Jeong, H. H. Lee, H. Yang, J. K. Kim, S. Okamoto, S. Aida, and S. Sakurai. Kinetics and mechanism of morphological transition from lamella to cylinder microdomain in polystyrene-block-poly(ethylene-co-but-1-ene)-*block*-polystyrene triblock copolymer, Macromolecules 36 (2003):1685-1693.

[15] S. Sakurai, H. Kawada, T. Hashimoto, and L. J. Fetters. Thermoreversible morphology transition between spherical and cylindrical microdomains of block copolymers, Macromolecules 26 (1993):5796-5802.

[16] S. Qi and Z.-G. Wang. Kinetic pathways of order-disorder and order-order transitions in weakly segregated microstructured systems, Phys. Rev. Lett. 76 (1996):1679-1682.

[17] D. A. Hajduk, R.-M. Ho, M. A. Hillmyer, F. S. Bates, and K. Almdal. Transition mechanisms for complex ordered phases in block copolymer melts, J. Phys. Chem. B 102 (1998):1356-1363.

[18] M. E. Vigild, K. Almdal, K. Mortensen, I. W. Hamley, J. P. A. Fairclough, and A. J. Ryan. Transformations to and from the gyroid phase in a diblock copolymer, Macromolecules 31 (1998):5702-5716.

[19] G. Floudas, R. Ulrich, and U. Wiesner. Microphase separation in poly(isoprene-*b*-ethylene oxide) diblock copolymer melts. I. Phase state and kinetics of the order-to-order transitions, J. Chem. Phys. 110 (1999):652-663.

[20] K. Kimishima, T. Koga, and T. Hashimoto. Order-order phase transition between spherical and cylindrical microdomain structures of block copolymer. I. Mechanism of the transition, Macromolecules 33 (2000):968-977.

[21] J.-F. Gohy, B. G. G. Lohmeijer, and U. S. Schubert. Reversible metallo-supramolecular block copolymer micelles containing a soft core, Macromol. Rapid Comm. 23 (2002):555-560.

[22] C.-Y. Wang and T. P. Lodge. Kinetics and mechanisms for the cylinder-to-gyroid transition in a block copolymer solution, Macromolecules 35 (2002):6997-7006.

[23] T. Q. Chastek and T. P. Lodge. Measurement of gyroid single grain growth rates in block copolymer solutions, Macromolecules 36 (2003):7672-7680.

[24] C. Lai, Y.-L. Loo, R. A. Register, and D. H. Adamson. Dynamics of a thermoreversible transition between cylindrical and hexagonally perforated lamellar mesophases, Macromolecules 38 (2005):7098-7104.

[25] D. A. Hajduk, P. E. Harper, S. M. Gruner, C. C. Honeker, G. Kim, E. L. Thomas, and L. J. Fetters. The gyroid: A wew equilibrium morphology in weakly segregated diblock copolymers, Macromolecules 27 (1994):4063-4075.

[26] B. J. Dair, A. Avgeropoulos, N. Hadjichristidis, M. Capel, and E. L. Thomas. Oriented double gyroid films via roll casting, Polymer 41 (2000):6231-6236.

[27] T. Honda and T. Kawakatsu. Epitaxial transition from gyroid to cylinder in a diblock copolymer melt, Macromolecules 39 (2006):2340-2349.

[28] M. Pinna and A. V. Zvelindovsky. Kinetic pathways of gyroid-to-cylinder transitions in diblock copolymers under external fields: cell dynamics simulation, Soft Matter 4 (2008):316-327.

[29] K. Schmidt, C. W. Pester, H. G. Schoberth, H. Zettl, K. A. Schindler, and A. Böker. Electric field induced gyroid-to-cylinder transitions in concentrated diblock copolymer solutions, Macromolecules 43 (2010):4268-4274.

[30] S. Park, D. H. Lee, J. Xu, B. Kim, S. W. Hong, U. Jeong, T. Xu, and T. P. Russell. Macroscopic 10-terabit-per-square-inch arrays from block copolymers with lateral order, Science 323 (2009):1030-1033.

[31] H. Jinnai, R. J. Spontak, and T. Nishi. Transmission electron microtomography and polymer nanostructures, Macromolecules 43 (2010):1675-1688.

[32] M. J. Fasolka and A. M. Mayes. Block copolymer thin films: physics and applications, Annu. Rev. Mater. Res. 31 (2001):323-355.

[33] W. Joo, H. J. Kim, and J. K. Kim. Broadband antireflection coating covering from visible to near infrared wavelengths by using multilayered nanoporous block copolymer films, Langmuir 26 (2009):5110-5114.

[34] A. C. Edrington, A. M. Urbas, P. DeRege, C. X. Chen, T. M. Swager, N. Hadjichristidis, M. Xenidou, L. J. Fetters, J. D. Joannopoulos, Y. Fink, and E. L. Thomas. Polymer-based photonic crystals, Adv. Mater. 13 (2001):421-425.

[35] V. N. Urade, T.-C. Wei, M. P. Tate, J. D. Kowalski, and H. W. Hillhouse.

Nanofabrication of double-gyroid thin films, Chem. Mater. 19 (2007):768-777.

[36] J. Jung, H.-W. Park, S. Lee, H. Lee, T. Chang, K. Matsunaga, and H. Jinnai. Effect of film thickness on the phase behaviors of diblock copolymer thin film, ACS Nano 4 (2010):3109-3116.

[37] M.-S. She, T.-Y. Lo, and R.-M. Ho. Controlled ordering of block copolymer gyroid thin films by solvent annealing, Macromolecules 47 (2014):175-182.

[38] Y.-H. Wu, T.-Y. Lo, M.-S. She, and R.-M. Ho. Morphological evolution of gyroid-forming block copolymer thin films with varying solvent evaporation rate, ACS Appl. Mater. Inter. 7 (2015):16536-16547.

[39] T.-Y. Lo, R.-M. Ho, P. Georgopanos, A. Avgeropoulos, and T. Hashimoto. Direct visualization of order-order transitions in silicon-containing block copolymers by electron tomography, ACS Macro Letters 2 (2013):190-194.

[40] T.-Y. Lo, A. Dehghan, P. Georgopanos, A. Avgeropoulos, A.-C. Shi, and R.-M. Ho. Orienting block copolymer thin films via entropy, Macromolecules 49 (2016):624-633.

[41] V. Abetz, N. Hadjichristidis, H. Iatrou, M. Pitsikalis, and P. F. W. Simon. Block copolymers I: Springer Berlin Heidelberg, 2005.

[42] H.-W. Park, K. Im, B. Chung, M. Ree, T. Chang, K. Sawa, and H. Jinnai. Direct observation of HPL and DG structure in PS-*b*-PI thin film by transmission electron microscopy, Macromolecules 40 (2007):2603-2605.

[43] I. Vukovic, T. P. Voortman, D. H. Merino, G. Portale, P. Hiekkataipale, J. Ruokolainen, G. ten Brinke, and K. Loos. Double gyroid network morphology in supramolecular diblock copolymer complexes, Macromolecules 45 (2012):3503-3512.

[44] S. Foerster, A. K. Khandpur, J. Zhao, F. S. Bates, I. W. Hamley, A. J. Ryan, and W. Bras. Complex phase behavior of polyisoprene-polystyrene diblock copolymers near the order-disorder transition, Macromolecules 27 (1994):6922-6935.

[45] J. Zhao, B. Majumdar, M. F. Schulz, F. S. Bates, K. Almdal, K. Mortensen, D. A. Hajduk, and S. M. Gruner. Phase behavior of pure diblocks and binary diblock blends of poly(ethylene)-poly(ethylethylene), Macromolecules 29 (1996):1204-1215.

[46] E. Huang, S. Pruzinsky, T. P. Russell, J. Mays, and C. J. Hawker. Neutrality conditions for block copolymer systems on random copolymer brush surfaces, Macromolecules 32 (1999):5299-5303.

[47] M. J. Maher, C. M. Bates, G. Blachut, S. Sirard, J. L. Self, M. C. Carlson, L. M. Dean, J. D. Cushen, W. J. Durand, C. O. Hayes, C. J. Ellison, and C. G. Willson. Interfacial design for block copolymer thin films, Chem. Mater. 26 (2014):1471-1479.

[48] I. Prasad, H. Jinnai, R.-M. Ho, E. L. Thomas, and G. M. Grason. Anatomy of triply-periodic network assemblies: characterizing skeletal and inter-domain surface geometry of block copolymer gyroids, Soft Matter 14 (2018):3612-3623.

[49] M. Imai, K. Sakai, M. Kikuchi, K. Nakaya, A. Saeki, and T. Teramoto. Kinetic pathway to double-gyroid structure, J. Chem. Phys. 122 (2005):214906.

[50] K. K. Tenneti, X. Chen, C. Y. Li, Y. Tu, X. Wan, Q.-F. Zhou, I. Sics, and B. S. Hsiao. Perforated layer structures in liquid crystalline rod-coil block copolymers, J. Am. Chem. Soc. 127 (2005):15481-15490.